ФИЗИКА ПРОЧНОСТИ И ПЛАСТИЧНОСТИ

Mechanical Testing of the Shape-Memory Materials Synthesized by a Plasma-Spark Method

G. E. Monastyrsky[*,**], A. V. Gilchuk[*], P. Ochin[***], O. M. Ivanova[****], Yu. N. Podrezov[****], and Yu. N. Koval[**]

[*]*National Technical University of Ukraine 'Kyiv Polytechnic Institute',
 37 Peremogy Prosp.,
 UA-03506 Kyiv, Ukraine*
[**]*G. V. Kurdyumov Institute for Metal Physics, N.A.S. of Ukraine,
 36 Academician Vernadsky Blvd.,
 UA-03680 Kyiv-142, Ukraine*
[***]*Institut de Chimie et des Matériaux Paris Est (ICMPE–CNRS),
 2–8 Rue Henri Dunant,
 94320 Thiais, France*
[****]*I. M. Frantsevich Institute for Materials Science, N.A.S. of Ukraine,
 3 Krzhizhanovsky Str.,
 UA-03680 Kyiv-142, Ukraine*

Compression tests are carried out at room temperature with the as-cast and spark-plasma sintered (SPS) specimens of $Ni49.0–Mn28.5–Ga22.5$ (at.%) and $Ni63–Al37$ (at.%) alloys. For both systems, ductility of the SPS compacts increases more than by one order of magnitude. Compressive strength of Ni–Mn–Ga alloy increases from 180–240 MPa for induction melted specimens to 510–815 MPa for spark-plasma sintered specimens, depending on the regimes of processing, and for Ni–Al alloy, from 760 to 1310 MPa. Fracture stress of Ni–Mn–Ga and Ni–Al specimens raise from 185–215 to 1170 MPa and from 790 to 1870 MPa, respectively. The SEM and XRD investigations reveal that sintered samples of both systems have a composite structure, which contains the micron-size metallic particles bound by the binder phase. This phase consists of Ni_3Al and Al_2O_3 phases in case of Ni–Al alloy and consists of MnO with apparently small amount of Ni_3Ga phase in case of Ni–Mn–Ga alloy. As assumed, this phase strengthens the grain boundaries. This one, in conjunction with reduction of the grain size, the manifold morphology of the Ni–Mn–Ga specimens consolidated from the hollow particles, the presence of extra ductile γ'-phase in Ni–Al particles, provides the enhancing mechanical properties of alloys fabricated by means of the SPS method.

Випробування на стиснення було виконано при кімнатній температурі

1547

для зразків стопів Ni49,0−Mn28,5−Ga22,5 (ат.%) та Ni63−Al37 (ат.%), як щойно витоплених, так і одержаних плазмово-іскровою методою (ПІМ). Для обох систем пластичність ПІМ-зразків зростає більш ніж на порядок порівняно із вихідними. Міцність на стиск стопу Ni−Mn−Ga збільшується від 180−240 МПа для щойно витоплених зразків до 510−815 МПа для ПІМ-зразків, залежно від режимів оброблення; для стопу Ni−Al — від 760 до 1310 МПа. Напруження руйнування зразків Ni−Mn−Ga збільшується від 185−215 до 1170 МПа, а для зразків Ni−Al — від 790 до 1870 МПа. Спечені зразки обох систем мають композитну структуру, утворену з металевих частинок мікронних розмірів, пов'язаних сполучною фазою, що складається з Ni_3Al і Al_2O_3 для стопу Ni−Al та з MnO з невеликою кількістю Ni_3Ga для стопу Ni−Mn−Ga. Передбачається, що ця фаза зміцнює межі зерен. Це разом із зменшенням розміру зерна, а також багатозв'язною морфологією зразків Ni−Mn-Ga, консолідованих із порожнистих частинок, та наявністю пластичної γ′-фази в частинках Ni−Al покращує механічні властивості стопів, одержаних плазмово-іскровою методою.

Испытания на сжатие были выполнены при комнатной температуре для образцов сплавов Ni49,0−Mn28,5−Ga22,5 (ат.%) и Ni63−Al37 (ат.%), как для выплавленных, так и полученных плазменно-искровым методом (ПИМ). Для обеих систем пластичность ПИМ-образцов возрастает более чем на порядок по сравнению с исходными. Прочность на сжатие сплава Ni−Mn−Ga увеличивается от 180−240 МПа для выплавленных образцов до 510−815 МПа для ПИМ-образцов в зависимости от режимов обработки, для сплава Ni−Al — от 760 до 1310 МПа. Напряжение разрушения образцов Ni−Mn−Ga увеличивается от 185−215 до 1170 МПа, а для образцов Ni−Al — от 790 до 1870 МПа. Спечённые образцы обеих систем имеют композитную структуру, образованную из металлических частиц микронных размеров, скреплённых связующей фазой, состоящей из Ni_3Al и Al_2O_3 для сплава Ni−Al и из MnO с небольшим количеством Ni_3Ga для сплава Ni−Mn−Ga. Предполагается, что эта фаза укрепляет границы зёрен. Это вместе с уменьшением размера зерна, а также многосвязной морфологией образцов Ni−Mn−Ga, консолидированных из полых частиц, и наличием пластической γ′-фазы в частицах Ni−Al улучшает механические свойства сплавов, полученных плазменно-искровым методом.

1. INTRODUCTION

Ni−Al intermetallics enriched with Ni are the promising shape-memory alloys. Currently, their practical application is limited by low room temperature plasticity of their polycrystalline forms, in particular due to large grain scales and the formation of brittle intermetallic compound Ni_5Al_3 during the preparation or heat treatment. Ni−Mn−

Ga alloys also have attracted considerable attention because of their potential as magnetically driven shape-memory alloys, high-temperature shape-memory alloys, vibration damping and magnetocaloric devices [1]. Significant brittleness of the Ni−Mn−Ga alloys is a serious problem hindering application of this material. Attractive perspectives of the practical applications of these materials stimulate the continuous searching for new routes of their elaboration.

Powder metallurgy technique is believed as good alternative for the ductility improvement. Among others, the spark-plasma sintering (SPS) method looks as express method allowing the sintering powders within several minutes in vacuum or inert gas atmosphere. In [2−7], the study of Ni−Mn−Ga alloys fabricated by the SPS method have been reported. Now, the data about plasticity of the SPS compacts are contradictory. In [7], authors have shown that the ductility in compressive tests of SPS compacts sintered at 1173 K followed by homogenization at 1073 K for 240 hours was about 14.2% in comparison with 1.5% for the arc-melted materials. Tien *et al.* have manifested in [4−6] that the ductility under similar conditions of SPS Ni−Mn−Ga alloys sintered from mechanically milled powders at 1173 K followed by homogenization at 1073 K for 12 hours was about 27%, while the ductility of arc-melted samples have achieved 8%. At the same time, the fracture strains of SPS compacts sintered from mechanically crashed strips of Ni−Mn−Ga was only about 1.5−3.3% [3]. Such discrepancy between the results presupposes the large sensitivity of the Ni−Mn−Ga ductility to the fabrication conditions as well as the materials used for the sintering.

In our previous communication [8], the results of spark-plasma sintering of Ni−Mn−Ga spark-erosion powder and the peculiarities of the martensitic transformation in compacts are described. As is shown, the morphology and microstructure of spark-erosion particles are very similar to gas atomized powders. It is important to compare the ductility of SPS compact elaborated from such particles with those ones fabricated from mechanically crashed materials.

There are a few communications concerning the elaboration of shape-memory Ni−Al alloys by SPS method within the authors' knowledge. All of them dealt with the consolidation from elemental Ni and Al powders [9−11]. No results of the ductility study are presented in them. The microstructure of Ni−Al shape-memory alloys consolidated by SPS method from pre-alloyed spark-erosion Ni−Al powders are presented in our previous communication [12]. The investigation of mechanical properties of Ni−Al SPS compacts has to be done.

The aim of current work is to compare the mechanical properties of the spark-plasma sintered Ni−Mn−Ga and Ni−Al compacts, both elaborated from spark-erosion powders, and to elucidate the peculiarities of the SPS microstructure, which could be affected by these properties.

2. EXPERIMENTAL

The route of the elaboration and thermal treatment of the spark-erosion powders with a nominal composition Ni49.0–Mn28.5–Ga22.5 (at.%) has described in details elsewhere [8, 12]. Alloy with a nominal composition Ni63–Al37 (at.%) were arc-melted and moulded into the bars with the diameter of 4 mm and the length of 12 cm. Part of the rods were used as electrodes for spark-erosion apparatus and the remaining were broken at 3–4 mm pieces (granules) and were used to obtain powder by spark-erosion method. The general principle of the spark-erosion processing is described in details in [13].

The SPS apparatus DR.SINTER® LAB Series is used for the sintering of both materials. Uniaxial pressure of maximum 99.5 MPa is applied for densification. About 1 g of powder was preliminary slightly compacted in the die, placed inside the working chamber and the system was evacuated. As a result, the compacts with a diameter of 8 mm and height of 4–6 mm were obtained. Certain part of both kinds of the powders was annealed in H_2 atmosphere before the spark-plasma sintering. The regimes of sintering and preliminary annealing of spark-erosion powders are listed in the Table 1 and Table 2.

XRD studies of the compacts are carried out at room temperature in Bragg–Brentano configuration with a $CoK_{\alpha_{1,2}}$ radiation. A PANalyticalX'Pert PRO diffractometer with a linear detector is used. The morphology and composition study of the sintered samples is analysed by JSM-6490LV or Auger spectrometer JAMP-9500F both equipped with EDX spectrometer INCA PentaFETx3. Compression testing is conducted at ambient temperature on a CERAMTEST machine at a strain rate of 0.3 mm/min using the induction-melted (Ni–Mn–Ga), arc-melted (Ni–Al) and sintered specimens with a rectangular shape of the typical dimensions $1.5 \times 1.5 \times 2.5$ mm^3.

TABLE 1. Mechanical properties of Ni–Al compacts (δ—deformation before fracture, $\sigma_{0.2}$—yield strength, σ_B—ultimate stress, ρ/ρ_{theor}—percentage of theoretical density).

Method	Annealing in H_2	$\sigma_{0.2}$	σ_B	δ	ρ/ρ_{theor}	Fracture mode
		MPa		%		
Arc melting	–	760	790	1.3	94.9	Breaking completely
SPS, 1000°C, 2 min	400°C, 1 h	970	1000	0.6	98.1	Breaking completely
SPS, 900°C, 4 min	–	1310	1810	7.7	93.0	Cracks
SPS, 1150°C, 20 sec	–	1165	1870	10.4	94.9	Cracks

TABLE 2. Mechanical properties of Ni−Mn−Ga compacts (δ—deformation before fracture, $\sigma_{0.2}$—yield strength, σ_B—ultimate stress, ρ/ρ_{theor}—percentage of theoretical density, LAr—liquid argon, LN—liquid nitrogen).

Method	Annealing in H_2	δ, %	$\sigma_{0.2}$, MPa	σ_B, MPa	ρ/ρ_{theor}, %	Fracture mode
Inducting melting		0.3	180−240	185−270	95.7	Breaking along grain boundaries
SPS, 700°C, 16 min, from SE powder obtained in LAr	Not annealed	3.5−4.5	580−590	695−775	93.5	Cracks, cleavages
	700°C	2.2−2.4	510−560	600−660	97.3	
	900°C	3.6	550	750	96.7	
SPS, 700°C, 16 min, from SE powder obtained in LN	Not annealed	0.4−2.1	715−735	740−830	97.4	
	700°C	3.7−4.1	770−815	1050−1060	95.5	
	900°C	6.0	660	1170	98.2	

3. RESULTS AND DISCUSSION

3.1. Phase Content of the Sintered Samples

XRD patterns (Fig. 1, *a*) have shown that Ni−Al SPS compacts contained mainly austenite β-phase [14] (B2 ordered), γ'-phase [15] ($L1_2$ ordered), 3R martensite phase [16, 17] ($L1_0$ ordered), and certain amount of α-Al_2O_3 alumina [18] independent from the elaboration and treatment conditions. The relative intensities of γ'-phase and α-Al_2O_3 alumina peaks are lower for the samples prepared from powders, preliminary annealed in H_2 atmosphere.

Phase content of Ni−Mn−Ga compacts is the same for all powders sintered at 700°C. Namely, the main phases, which has been found, are non-modulated tetragonal martensite [19] ($L1_0$ ordered), cubic γ-MnO [20], certain amount of 14M martensite [19], and small amount of austenitic $L2_1$ ordered phase [21]. In addition, several weak peaks could be attributed to α-Mn [22]. Four lines of cubic Ni_3Ga [23] (space group $Pm-3m$) appeared in spectra, however, no superlattice reflexes were found. Thus, it can be attributed to γ-phase. The intensities of these reflexes are especially significant for the samples prepared from as received powder into liquid nitrogen (LN) environment. The XRD results
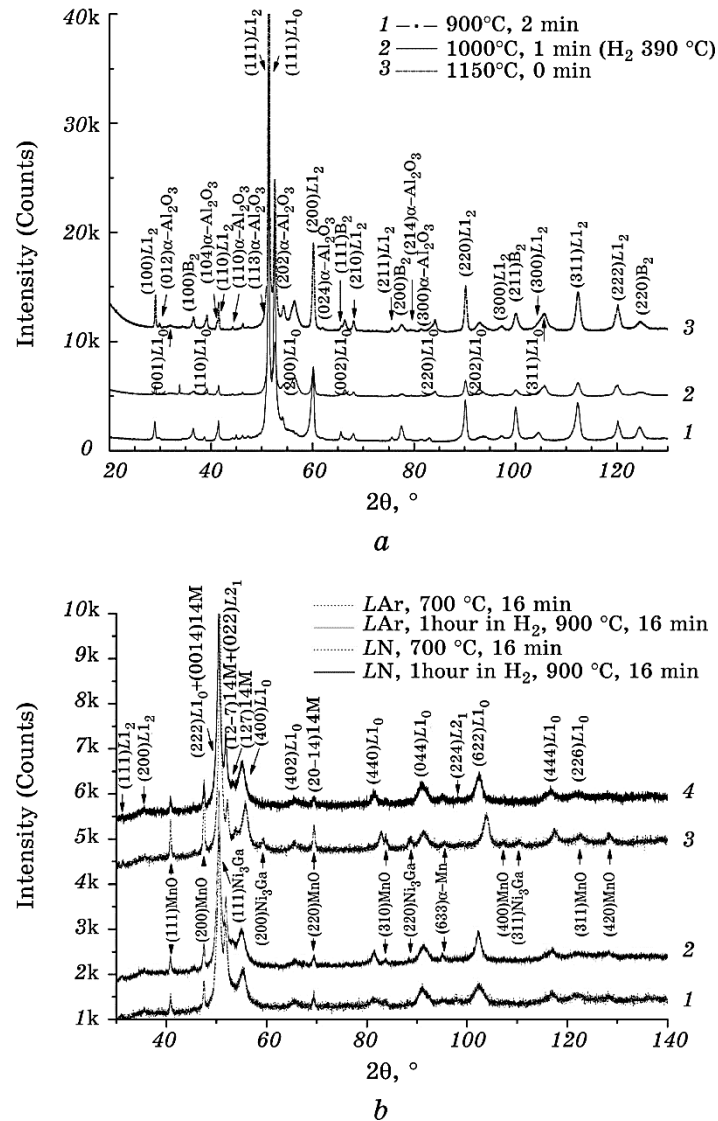
Fig. 1. XRD spectra of SPS samples: *a*—Ni–Al, *b*—Ni–Mn–Ga. Strongest line of NM, 14M martensite, α-Mn and Ni_3Ga overlap each other at $\cong 51°$.

show that samples of both compositions contain not only main austenitic and martensitic phases as well as that expected from corresponding phase diagram (γ'-phase or Ni_3Al), but extra phases including oxides.

The appearance of these phases seems to be connected with the mechanism of sintering and interaction between the elemental powders and their oxides contained in nanofraction of spark-erosion powders [24].
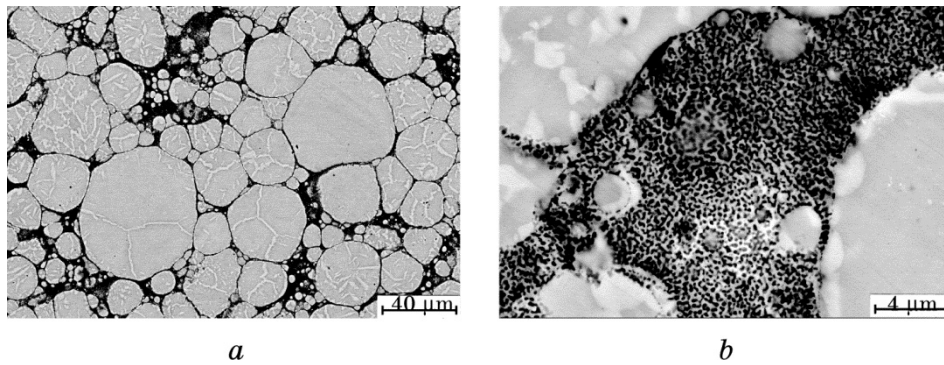
Fig. 2. Microstructure of the Ni−Al compacts sintered at 1150°C from the as-received powder: *a*—BSE image of the several decades micron sized particles embedded into the binder phase; Ni_3Al phase appears as light grey precipitations, which decorate the grains boundaries inside the micron sized particles; *b*—enlarged BSE image of the binder fraction.

3.2. Microstructure of the Sintered Samples

SEM investigation has revealed the composite structure of both materials after consolidation. Namely, the several decades micron sized particles (Figs. 2, *a*, 3, *a*, and 4) have bound by the binder fraction, which appears as the interlaced and twisted submicron or even nanoscale black and white precipitates (Figs. 2, *b*, 3, *b*, and 4). Taking into account the XRD data, one can suppose that the large particles consist of the austenitic and martensitic phases mainly, while interparticle phases formed binder fraction is the complex mixture of interme-
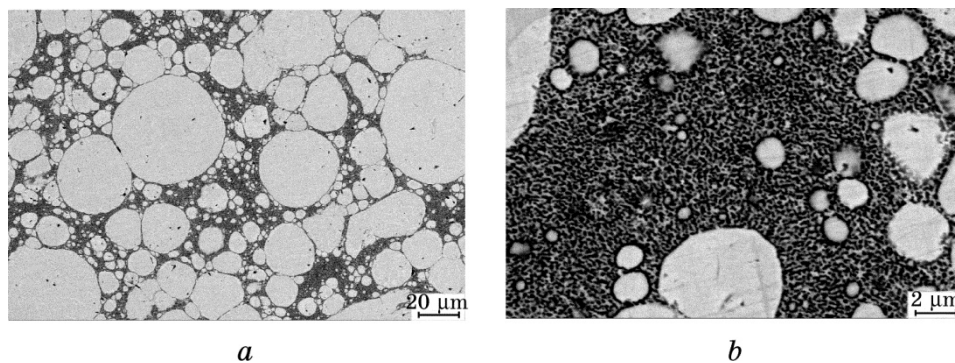

Fig. 3. Microstructure of the Ni−Al compacts sintered at 1000°C from the powder annealed in hydrogen gas atmosphere at 390°C: *a*—BSE image of the several decades micron sized particles embedded into the binder fraction; *b*—enlarged BSE image of the binder fraction.
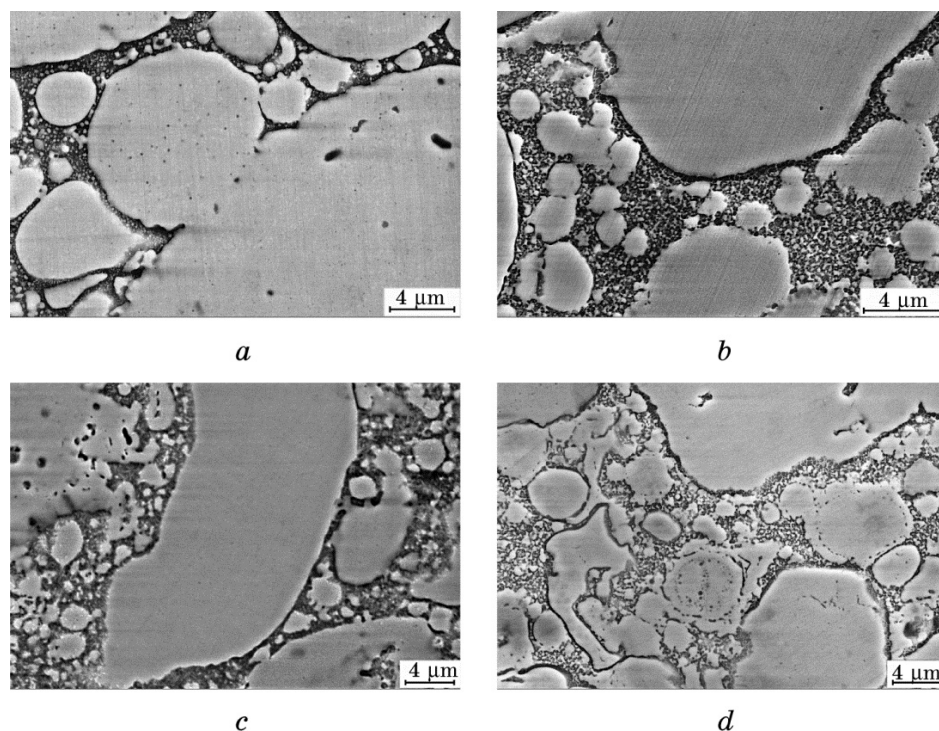
Fig. 4. Microstructure of the binder phase (SE images) of the Ni–Mn–Ga compacts sintered from the powders obtained in liquid argon (*a*, *b*) and liquid nitrogen (*c*, *d*). Compacts were sintered at 700°C from the as-received powders (*a*, *c*) and those ones annealed in hydrogen gas atmosphere at 700°C (*b*, *d*).

tallic phases and oxides. Indeed, the comparison the BSE images of Ni–Al compacted from as prepared (Fig. 2) particles with those produced from pre-annealed in hydrogen atmosphere particles (Fig. 3) shows that Ni_3Al phase appears as light grey precipitations in micron sized particles in former case, while the amount of this phase is lesser in latter case. At the same time, reflexes of Ni_3Al phase appear on X-ray spectrum of the sample consolidated from the pre-annealed in hydrogen atmosphere particles (Fig. 1, *a*, spectrum 2). Thus, one can assume that the interparticle phase is some kind of cermet consisting of Ni_3Al and Al_2O_3 phases. In case of Ni–Mn–Ga, the fine structure of binder interparticle phase is very similar to that observed in Ni–Al (Fig. 4, *b*, *d*). Taking into account X-ray data, one can assume that it is also cermet consisting mainly of MnO and apparently small amount of Ni_3Ga phase.

The effect of preliminary annealing on the microstructure is completely different for Ni–Al and Ni–Mn–Ga systems. Comparison of Figs. 2 and 3 shows that 'black' component in binder fraction of Ni–Al

obtained from preliminary annealing powders represent more noticeably. This component is presumably aluminium oxide although the porous structure of binder fraction cannot be excluded too. Contrary, the most noticeable structure of binder phase formed from interlaced and twisted black and white precipitates appears in Ni–Mn–Ga samples consolidated from annealed in hydrogen atmosphere particle.

3.3. Mechanical Compressive Tests

In order to investigate the ductility of the spark-plasma sintered and as-cast specimens, the compression tests were carried out at room temperature. All specimens were compressed to the fracture. The results of compression tests are presented in Table 1 and Table 2. The compressive stress–strain curves obtained from the sintered specimens in comparison with that from the as-cast specimen are shown on Fig. 5. It can be seen that the as-cast specimens for both systems are subjected to very low fracture strains. The induction melted Ni–Mn–Ga specimens were broken along the boundaries of 0.5–3 mm sized grains, which have elongated shape due to the casting in the mould. Ni–Al arc-melted specimens were subjected to a larger contraction before breaking and demonstrate both intercrystalline and transcrystalline fracture modes (Fig. 6, *a*) with the typical martensitic lamellar substructures inside the grains. In both cases, $\sigma_{0.2}$ (yield strength) practically coincides with σ_B (ultimate stress). It indicates the brittle nature of as-cast specimens that makes possible their fracture before (or simultaneously with) the visible yielding.

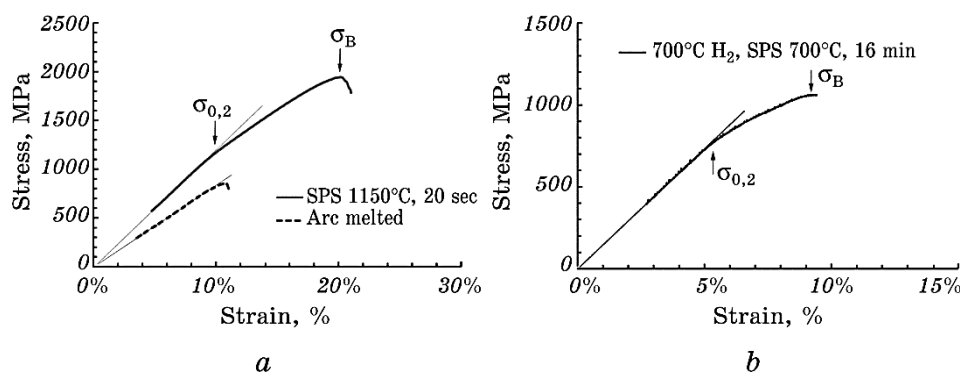In almost all sintered compacts for both systems, the fracture oc-

Fig. 5. Typical stress–strain curves after compression tests for the Ni–Al (*a*) and Ni–Mn–Ga (*b*) SPS compacts; $\sigma_{0.2}$ was determined as a stress, under which the deflection from straight 'elastic' line appears, σ_B corresponds to the maximum on the stress–strain curve.
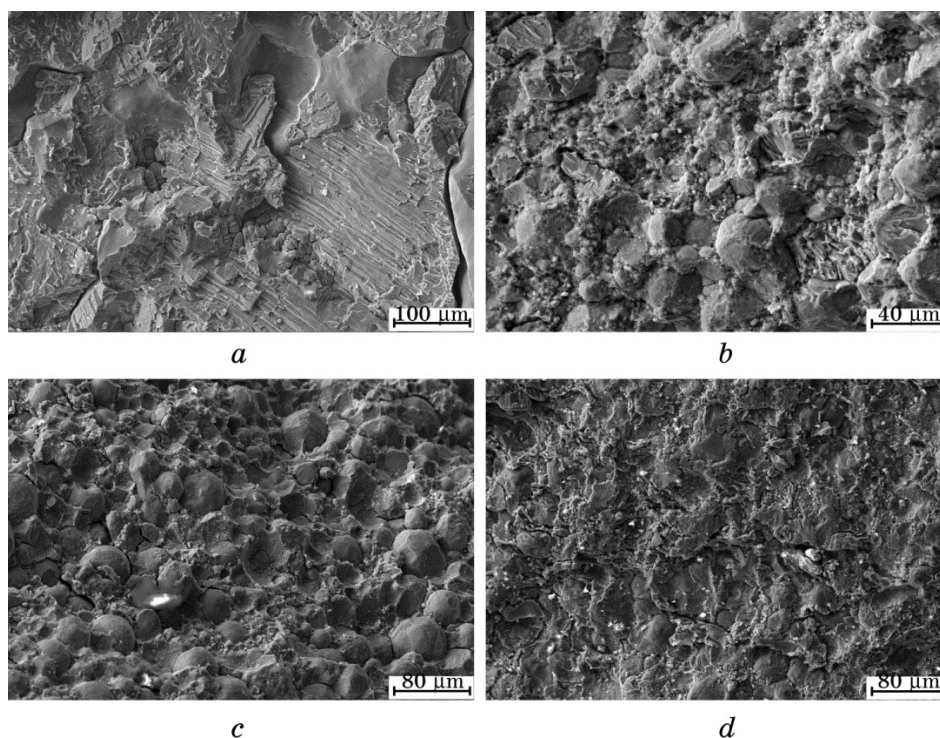
Fig. 6. Scanning electron micrographs showing the compression fracture morphology of: Ni–Al arc-melted specimen (*a*) and Ni–Al compact sintered at 1150°C from the as-received powder (*b*); Ni–Mn–Ga compacts sintered at 700°C from the powders obtained in liquid argon (*c*) and liquid nitrogen (*d*). The powders were preliminary annealed in hydrogen gas atmosphere at 700°C.

curred at the strains more than in one order larger those in as-cast specimens. The compressive yield strength and fracture stress for the sintered specimens are also significantly higher. This drastic increase of compressive strength and fracture stress is especially clear seen in Ni–Mn–Ga consolidated compacts. This demonstrates that compressive ductility for Ni–Mn–Ga and Ni–Al alloys is significantly enhanced by the SPS technique. The enhancement of the mechanical properties in compressive test for the sintered specimens may be attributed to a) the strengthening of grain boundaries, b) the reduction of the grain size, c) the morphology of the sintered specimens, d) the formation extra ductile phases during SPS, e) the effect of residual porosity and f) martensite detwinning process.

Since the stress plateau, corresponding to the reorientation of martensite variants, is not evident in the stress–strain curves (Fig. 5), one can suggest that the deformation is mainly caused by the dislocation mechanisms rather than the martensite detwinning process. The con-

tribution of residual porous collapse mechanism in the specimen deformation can be estimated according to the relation $(100 - \rho/\rho_{\text{theor}})/3$. Using the data from Table 1 and Table 2, one can see that this contribution, if exist, is not sufficient to explain the deformation before fracture for the most specimens.

According to the Hall–Petch relationship, the reduction of grain size leads to the increase of compressive strength rather than to ductility. In turn, higher strength is achieved with the loss of plasticity in general but not in the current case. The reasons can be different for the Ni–Mn–Ga and Ni–Al systems.

There are some indirect evidences of the ductility enhancing for the spark-plasma sintered Ni–Mn–Ga [4, 5, 7], which was related by authors to the grain size reduction. In [6], authors claimed that the sintered specimen with optimal grain size of 34 μm exhibits the highest fracture strain of 29%; however, no explanation of grain size effect was given. As it is seen from Table 2, the refining of grain structure causes the increase in the compression strength (the finer grains were observed for SPS specimens sintered from the powder obtained in liquid nitrogen). However, the result of strengthening is opposite for the samples prepared from preliminary annealed in hydrogen atmosphere particles and from those without annealing. It suggests that other factors should be taken into account. One of them is the strengthening due to intergranular binder phase. It seems the binder phase effectively hinders the movement of dislocation and the crack propagation until the loading stresses overcome the adhesive forces between the Ni–Mn–Ga microns sized particles and binder fraction. After that, the breaking of sample is going on through the boundary of the particles. The fracture surfaces, which show a mixture of dimples and bulges or swellings (Fig. 6, *c*), confirms this assumption. The manifold morphology (Fig. 4, *c*, *d*) of Ni–Mn–Ga SPS specimens sintered from the hollow particles spark-eroded in liquid nitrogen influences also the fracture surface. It is less roughness, and the tearing ridges are observed (Fig. 6, *d*). These morphological peculiarities enhance the compressive strength and fracture stress as well as contraction before fracture.

For the Ni–Al, the consensus of many long term investigations concerning the lack of room temperature ductility in Ni–Al compound is that the number of available independent slip systems is insufficient (only 3 for {110}(100) slip). Therefore, the von Mises criterion for plasticity [24]—at least, five independent slip systems in a grain—is not fulfilled, and Ni–Al polycrystals are expected to be brittle. One of the approaches to increase the number of operative slips systems is the grain size refining, which provides the high strength of the material. In that case, as it was shown in [25], fine grained structure of mechanically alloyed Ni–Al alloys allows to increase the stress to propagate cracks, whereas the high yield strength is sufficient to activate addi-

tional {110} (110) slip and fulfil the von Mises criterion. Another option, which is alternative to the above-mentioned mechanism of strengthening, is the action of the intergranular binder phase that is presumably cermet consisting of Ni_3Al and Al_2O_3 phases. Indirect evidence of this assumption is the nil ductility and smallest strength of Ni−Al SPS specimens sintered from the powders preliminary annealed in hydrogen atmosphere. As it is seen from Fig. 1, *a* (spectrum 2) for this treatment, the peaks of Ni_3Al and Al_2O_3 phases are low-level in comparison with those for other regimes of processing. It seems that adhesive forces between micron-size Ni−Al particles and binder fraction are small, and specimen is broken before yielding. Finally, enhancing ductility of Ni−Al SPS samples elaborated from not annealed powder can be partially attributed to the presence of γ′-phase. The ductility of γ′-phase is much better than β-phase and martensitic phase that is ordinary used for the improvement of mechanical properties of Ni−Al alloys.

4. CONCLUSIONS

The microstructure of Ni49.0−Mn28.5−Ga22.5 (at.%) and Ni63−Al37 (at.%) spark-plasma sintered compacts consolidated from spark-erosion powders consists of the micron and submicron metallic particles bound by the binder phase. This phase can be considered as some kind of cermet consisting of the Ni_3Al and Al_2O_3 phases in case of Ni−Al alloy and of MnO with apparently small amount of Ni_3Ga phase in case of Ni−Mn−Ga alloy. Compression tests carried out at room temperature with the as-cast and spark-plasma sintered specimens evidently demonstrates that mechanical properties of materials are significantly enhanced by the SPS technique: the ductility increases in more than one order, the yield strength and ultimate stress are raised in more than a few times. This enhancement may be attributed to the strengthening of grain boundaries, caused by the action of the binder cermet phases, the reduction of the grain size, the manifold morphology of the Ni−Mn−Ga specimens consolidated from the hollow particles and causes the formation of extra ductile γ′-phase in Ni−Al particles during SPS.

REFERENCES

1.   O. Söderberg, Y. Ge, I. Aaltio, O. Heczko, and S.-P. Hannula, *Mater. Sci. Eng.*, **A481−482**: 80 (2008).
2.   Z. Wang, M. Matsumoto, T. Abe, K. Oikawa, J. H. Qiu, T. Takagi, and J. Tani, *Mater. Trans.*, **40**: 389 (1999).
3.   O. Söderberg, D. Brown, I. Aaltio, J. Oksanen, J. Syrén, H. Pulkkinen, and S.-P. Hannula, *J. Alloys Compd.*, **509**: 5981 (2011).

4. X. H. Tian, J. H. Sui, X. Zhang, X. Feng, and W. Cai, *Chin. Phys. B*, **20**, No.4: 047503 (2011).
5. X. H. Tian, J. H. Sui, X. Zhang, X. Feng, and W. Cai, *J. Alloys Compd.*, **509**: 4081 (2011).
6. X. H. Tian, J. H. Sui, X. Zhang, X. H. Zheng, and W. Cai, *J. Alloys Compd.*, **514**: 210 (2012).
7. Z. Wang, M. Matsumoto, T. Abe, K. Oikawa, T. Takagi, J. Qiu, and J. Tani, *Mater. Trans.*, **40**, No.9: 871 (1999).
8. P. Ochin, A. V. Gilchuk, G. E. Monastyrsky, Yu. N. Koval, A. A. Shcherba, and S. N. Zaharchenko, *Mater. Sci. Forum*, **738−739**: 451 (2013).
9. O. C. Alonso, J. G. Cabacas-Moreno, J. J. Cruz-Rivera, H. A. Calderyn, M. Umemoto, K. Tsuchiya, S. Quintana-Molina, and C. Falcony, *J. Metastable and Nanocrystalline Materials*, **8**: 635 (2000).
10. J. S. Kim, S. H. Jung, Y. Do Kim, C. H. Lee, and Y. S. Kwon, *Mater. Sci. Forum*, **449−452**: 1101 (2004).
11. J. S. Kim, H. S. Choi, D. V. Dudina, J. K. Lee, and Y. S. Kwon, *Solid State Phenom.*, **119**: 35 (2007).
12. G. E. Monastyrsky, P. A. Yakovenko, V. I. Kolomytsev, Yu. N. Koval, A. A. Shcherba, and R. Portier, *Mater. Sci. Eng. A*, **481−82**: 781 (2008).
13. J. Carrey, H. B. Radousky, and A. E. Berkowitz, *J. Appl. Phys.*, **95**: 823 (2004).
14. D. B. Miracle, *Acta Metall. Mater.*, **41**, No. 3: 649 (1993).
15. P. V. Mohan Rao, K. Satyanarayana Murthy, S. V. Suryanarayana, and S. V. Nagnder Naidu, *phys. status solidi (a)*, **133**: 231 (1992).
16. S. Rosen and J. A. Goebel, *Trans. Metall. Soc. AIME*, **242**: 722 (1968).
17. K. Enami, S. Nenno, and K. Shimizu, *Trans. Jap. Inst. Metals*, **14**: 161 (1973).
18. E. N. Maslen, V. A. Streltsov, N. R. Streltsova, N. Ishizawa, and Y. Satow, *Acta Crystallogr. Sec. B: Structural Science*, **49**: 973 (1993).
19. J. Pons, V. A. Chernenko, R. Santamarta, and E. Cesari, *Acta Mat.*, **48**: 3027 (2000).
20. C. A. Barrett and E. B. Evans, *J. Am. Ceram. Soc.*, **47**: 533 (1964).
21. P. J. Webster, K. R. A. Ziebeck, S. L. Town, and M. S. Peak, *Philos. Mag. B*, **49**: 295 (1984).
22. J. S. Kasper and B. W. Roberts, *Phys. Rev.*, **101**: 537 (1956).
23. Y. Mishima, S. Ochiai, and T. Suzuki, *Acta Metall.*, **33**: 1161 (1985).
24. G. E. Monastyrsky, P. Ochin, A. V. Gilchuk, V. I. Kolomytsev, and Yu. N. Koval, *J. Nano- and Electronic Physics*, **4**: 01007-1 (2012); R. von Mises, *Z. Angew. Math.*, **8**: 161 (1928).
25. S. Dymek, M. Dollar, S. J. Hwang, and P. Nash, *Mater. Sci. Eng. A*, **152**: 160 (1992).